PNAS RESEARCH ARTICLE | BIOPHYSICS AND COMPUTATIONAL BIOLOGY
PLANT BIOLOGY

Stomatal patchiness and cellular computing

David Peak[a,1], Matthew T. Hogan[b], and Keith A. Mott[c]

Edited by Stephen Long, University of Illinois at Urbana Champaign, Urbana, IL; received November 28, 2022; accepted March 1, 2023

Control of carbon dioxide and water vapor exchange between a leaf's interior and the surrounding air is accomplished by variations in the turgor pressures in the small epidermal and guard cells that cover the leaf's surface. These pressures respond to changes in light intensity and wavelength, temperature, CO_2 concentration, and air humidity. The dynamical equations that describe such processes are formally identical to those that define computation in a two-layer, adaptive, cellular nonlinear network. This exact identification suggests that leaf gas-exchange processes can be understood as analog computation and that exploiting the output of two-layer, adaptive, cellular nonlinear networks might provide new tools in applied plant research.

stomata | dynamics | computation

Significance

Stomata are variable aperture pores that allow carbon dioxide to enter a plant leaf to participate in photosynthesis, while simultaneously controlling water loss due to evaporation. This paper shows that the stomatal balancing act is described by a set of dynamical equations whose form is identical to that of the equations describing the currents and voltages in a "two-layer, adaptive, cellular nonlinear network" that computes. When appropriately parameterized such a network can computationally model a variety of plant attributes for different environmental conditions. Such computational experiments, varying the "plant" input parameters, hold the potential for suggesting genetic or environmental modifications that, in the real world, might lead to improved plant productivity.

"Emergent computation" (1, 2) is a form of problem-solving that results from the collective activity of a system of functional units, but in which there is no central unit capable of coordinating the behavior of the others. Leaderless, distributed problem-solving is a fundamental characteristic of biological organisms and also of various biomimetic computational networks. This fact leads to the speculation that some forms of biology and computation are closely allied. Often plants have been suggested as possible examples of such biological-computational systems (3–7), including noting the similarity of leaf dynamical processes to artificial cellular automata (8, 9). These proposed examples typically have not included a precise definition of the computational scenario the plant system is supposed to manifest. In this paper, on the other hand, the *structure and biological function* of a collection of stomata on the surface of a plant leaf are shown to be formally identical to the *structure and computational function* of a two-layer, adaptive, cellular nonlinear network (10).

The argument for this connection utilizes a theoretical model that incorporates biologically relevant structures and interactions to explain how stomatal apertures can collectively adjust to external stimuli. The biological relevance of the model is demonstrated in the following by comparing the model's outputs to well-known experimental results. The model is subsequently identified, feature-by-feature, with that of an actual, hardware, computational system. It is therefore proposed that the manipulation of water resources by (at least some) plants is equivalent to a specific form of *analog* computation. This identification holds the potential that such computation can suggest new methods for producing desirable plant attributes.

1. Elements of the Stomatal Network Model (the SNM)

The waxy epidermis of a plant leaf prevents massive water loss due to evaporation from the leaf's interior. In order for photosynthesis to proceed, the epidermis is perforated by stomata—small, variable-aperture openings that allow carbon dioxide to enter the leaf from the surrounding air. When open, stomata also allow water vapor to escape. So, stomatal aperture varies with changing external conditions to acquire sufficient carbon dioxide for photosynthesis while simultaneously preventing desiccation. This feat is accomplished by a pair of small "guard" cells that define the stomatal opening pushing against much larger "epidermal" cells in which they are embedded. The mechanical forces required for this process result from turgor pressure differences, within the respective cells, that are controlled by water transport into and out of the cells.

Essential for identifying a biological stomatal system with a relevant computational hardware system is the recognition that stomata at different places on a leaf interact with one another. For example, experiments in which a single stoma responds to a localized perturbation—such as by blowing dry air on it with a micropipette—show that many surrounding stomata also quickly respond (11). Perhaps more convincing support for stomatal interaction is the ubiquitous phenomenon of "stomatal patchiness," in which large regions of similar stomatal openness appear to sweep coherently over the surface of

Author affiliations: [a]Physics Department, Utah State University, Logan, UT 84322-4415; [b]Physics and Astronomy Department, University of Utah, Salt Lake City, UT 84112-0830; and [c]Biology Department, Utah State University, Logan, UT 84322-0300

Author contributions: D.P. and K.A.M. designed research; D.P., M.T.H., and K.A.M. performed research; and D.P. wrote the paper.

The authors declare no competing interest.

This article is a PNAS Direct Submission.

[1]To whom correspondence may be addressed. Email: david.peak@usu.edu.

Published March 27, 2023.

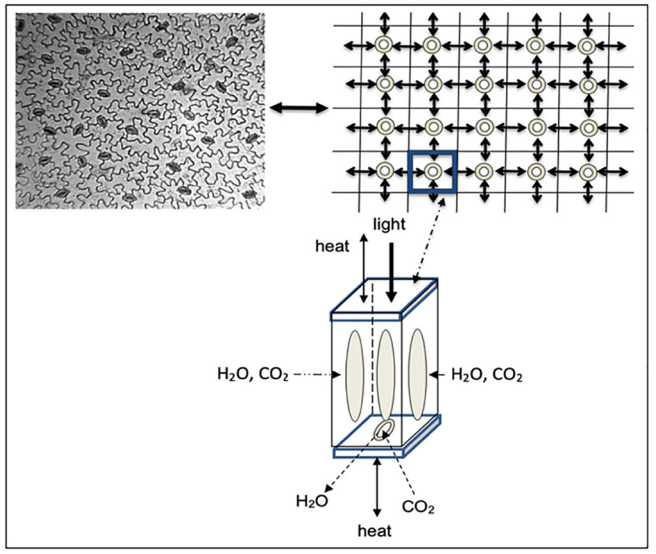

Fig. 1. Stomata on a leaf modelled as a network of plugs.

a leaf (8, 12). Stomata are not autonomous. The simplest explanation for their interaction is water exchange between adjacent epidermal cells, but in any case, stomata are locally interconnected in a type of organic network.

1.1. The Stomatal Unit. The proposed SNM assumes the leaf is hypostomatous, i.e., with stomata on the under (abaxial) side only. Often real stomata are roughly regularly distributed. (See the top leftmost image in Fig. 1; in it, stomata are "bean-shaped" and epidermal cells are shaped like jigsaw puzzle pieces.) For simplicity, the SNM treats adjacent stomata as evenly spaced and the leaf is envisioned as a regular array of identical, densely packed, rectangular-solid shaped plugs (top rightmost image). In the SNM, each plug has square epidermal caps on top and bottom, with mesophyll tissue filling the interior (lower image). Each abaxial cap in the model contains one stoma, a variable aperture pore.

Such a plug is defined as a "stomatal unit." The center of each stomatal unit is located at the site $r = (i, j)$ on a square grid, where i and j are integers.

Subsections (2.3)–(2.5) which follow briefly discuss experimentally-informed details of the structure and dynamics associated with the SNM. Subsequently, subsection (2.6) shows that the SNM's dynamic output closely agrees with observed stomatal behaviors.

1.2. Energy Fluxes. As illustrated in Fig. 1, light energy passing through the top (adaxial) cap of each stomatal unit is partially absorbed in the unit's mesophyll. Both caps also exchange thermal energy with the surrounding air.

1.3. Liquid Water. Liquid water flows from the plant's roots (or the leaf's petiole) to the mesophyll cells in the interior of the leaf. Epidermal cells on the abaxial surface of a stomatal unit exchange liquid water directly with the surfaces of the unit's mesophyll cells and also with the interiors of other abaxial epidermal cells in adjacent units.

1.4. Water Vapor and Carbon Dioxide. Saturated water vapor evaporating from the surfaces of mesophyll cells fills the leaf interior.

Stomatal guard cells exchange their internal liquid water with the water vapor in the adjacent "stomatal cavity," the region in the unit's interior close to the stomatal cap. When the stomatal pore is open, water vapor escapes the leaf and carbon dioxide enters the leaf interior and is absorbed in the mesophyll in the process of photosynthesis.

1.5. Dynamics.

1.5.1. The Stomatal Aperture. The instantaneous turgor pressure, $P_g(r, t)$, in the guard cells at site r and time t is assumed to be the same in both cells. If that pressure is sufficiently large to overcome $P_e(r, t)$, the instantaneous turgor pressure in the surrounding epidermal cells, that stoma opens. The instantaneous aperture of the opening, in the SNM, is proportional to the weighted difference, $P_g(r, t) - mP_e(r, t)$, in which the dimensionless factor m is related to the "mechanical advantage" of the larger epidermal cells over the smaller guard cells. The water vapor conductance associated with this stomatal aperture (13) is

$$g_{Sw}(r, t) = h\left\{ \chi(r)\left[P_g(r, t) - mP_e(r, t)\right]\right\}. \qquad [1]$$

In Eq. **1**, h is a dimensionless trilinear function of its argument: that is, the conductance i) is 0 if the argument is negative; ii) equals $g_{Sw,\,max}$ if the argument exceeds some maximum value; and iii) is just $\chi(r)\left[P_g(r, t) - mP_e(r, t)\right]$, otherwise. The positive coefficient $\chi(r)$ is related to the elasticity of the cells; it is assigned a slightly different random value at every site to account for the irregular packing of the epidermal cells. When $0 < g_{Sw}(r, t) < g_{Sw,max}$,

$$\frac{dg_{Sw}(r, t)}{dt} = \chi(r)\left[\frac{dP_g(r, t)}{dt} - m\frac{dP_e(r, t)}{dt}\right]. \qquad [2]$$

1.5.2. Summary of the Dynamics. The Appendix, section 3 below, contains the many details of how, in the SNM proposed here, the instantaneous cellular turgor pressures in Eq. **1** are related to external light intensity, humidity, temperature, and carbon dioxide concentration. In the following, the dynamical model resulting from these details is used to test the hypothesis that real stomatal networks might "compute." To accomplish this, the SNM equations are first shown to appropriately describe examples of observed stomatal behavior. Following that, the theoretical stomatal network architecture and function is shown to be identical to that of a computational network.

After aggregating the various pieces of the SNM developed in the Appendix, the relevant equations for the rates of change of the epidermal and guard cell pressures (and thus of the stomatal apertures) in Eq. **2** become respectively

$$dP_e(r, t)/dt = -\lambda_e P_e(r, t) + \lambda_e\left\{ -\rho E(r, t) + \Gamma_e(r, t)RT(r, t) + \eta_{ee}\sum_{r'}\left[P_e(r', t) - \Gamma_e(r', t)RT(r', t)\right]\right\}, \qquad [3a]$$

$$dP_g(r, t)/dt = -\lambda_g P_g(r, t) + \lambda_g\left[\Gamma_g(r, t)RT(r, t) + \frac{RT(r; t)}{V_W}\ln\left(\frac{w_c(r, t)}{w_m(r, t)}\right)\right]. \qquad [3b]$$

Here in Eq. **3a**: $E(r,t)$ is the evaporative flux from, and $T(r,t)$ is the temperature throughout, the plug at site r and time t; ρ is the resistance to liquid water flow from the roots (or petiole) to the leaf; λ_e and λ_g are rate constants for water transport in-and-out of the respective cell types; $\Gamma_e(r,t)$ and $\Gamma_g(r,t)$ are dissolved ion concentrations in the respective cells; η_{ee} measures the strength of water sharing between adjoining epidermal cells. In addition, in Eq. **3b**: V_W is the molar volume of water; the w variables are water vapor mole fractions in the stomatal cavity (c) and at the mesophyll (m); and the sums are over the nearest neighbors of the plug at r. In both equations R is the universal gas constant.

1.6. Comparing Example Output of the SNM with Experimental Results. In real plants, neighboring stomata typically differ somewhat in orientation and shape (see Fig. 1, for example). In the example simulations that follow (produced by integrating Eq. **2** after inserting Eqs. **3a** and **3b**), the small random variability in $\chi(r)$ generates small—calculated—aperture fluctuations. As shown below, the assumed random variability of stomatal units leads to insight into leaf phenomena that models based on identical stomata cannot address.

The example SNM results shown below all agree with known stomatal phenomena. These results are not individually "put in" with different parameters for each different example. All arise after iteratively adjusting the model parameters so that the various outputs for the different external conditions—*using a single set of parameter values*—mimic typical experimental observations found in many species.

1.6.1. *Stomatal Patchiness.* Often experiments examining stomatal behavior start with a leaf in the dark. When illumination is first turned on, high-resolution thermal imaging initially shows small, randomly positioned, temperature variations over the leaf's surface. After some minutes pass, these small fluctuations often grow into large patches of stomata in which similar warmer temperatures abut other large patches of stomata with similar cooler temperatures. This is the phenomenon of "stomatal patchiness" mentioned previously; it has been identified in hundreds of species in both the laboratory and the wild (14). Patchiness does not occur in the SNM if there is no random variability among the stomatal units.

Patchiness seems to suggest irregular, perhaps suboptimal, stomatal behavior—so, its ubiquity is puzzling. Nonetheless, the generation of patchiness is an essential first test that any plausibly correct model of stomatal arrays *must* pass. Fig. 2 shows simulations using Eqs. **2**, **3a**, and **3b**. Patchiness arises spontaneously in the SNM by water exchange wherever, in the initial configuration, small clusters of stomatal units with similar water potential are adjacent to clusters of units with a different (but similar-to-one-another) water potential.

The assumed small random variations in the simulated initial configuration produce, in the left image of Fig. 2, small random initial temperature fluctuations—shown as white for "warm" and black for "cool." Several calculated "minutes" later, depicted on the right in Fig. 2, the initial fluctuations have organized into much larger patches of warm and cool, similar to what is observed in experiments with real plants.

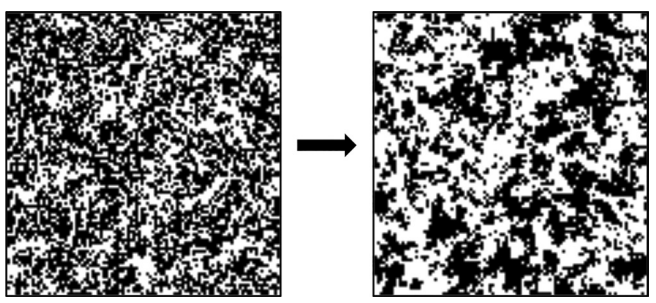

Fig. 2. Time development of simulated leaf surface temperature.

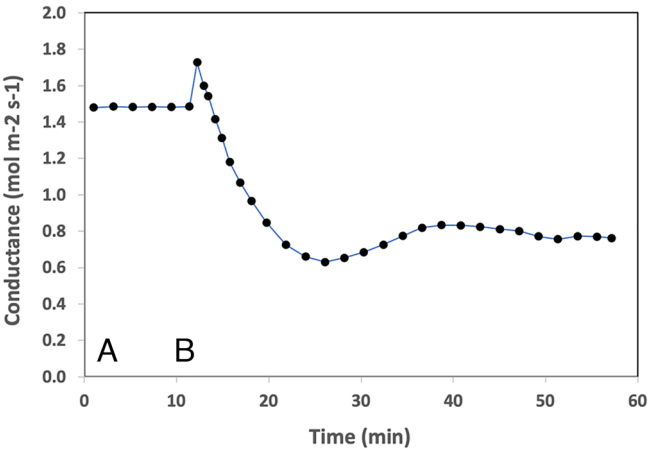

Fig. 3. Simulation of the "wrong-way" response.

The following simulations are equivalent to what would be inferred from gas exchange measurements, that is, stomatal behavior averaged over a large area of leaf in a gas exchange chamber.

1.6.2. *The Wrong-Way Response.* When humidity in the air surrounding an illuminated biological leaf is gradually lowered the leaf's stomata tend to gradually close. If the humidity drop is rapid, however, sometimes the stomata are observed to at first briefly open before closing. This is the "wrong-way response," which is observed in many experiments (15).

Fig. 3 shows a simulation with the SNM of a rapid humidity drop experiment. Between times "A" and "B" in the figure, the "leaf" has a large, steady, average stomatal aperture. At "B" the simulated external humidity is suddenly reduced. The immediate response is that the stomata open—i.e., respond the "wrong way"—after which the stomata close, as expected, with eventually a smaller average aperture. The wrong way response occurs in the SNM because epidermal cells are assumed to shed water faster than guard cells (i.e., because $\lambda_e > \lambda_g$) when humidity decreases.

1.6.3. *Red and Blue Light.* When real plants, with already open stomata, are suddenly exposed to bright monochromatic red light their stomata often begin a long duration episode of large amplitude oscillations. When low-intensity blue light is combined with the red, however, the oscillations are often observed to eventually damp out (16). Fig. 4 shows that this effect arises naturally in the SNM.

At first, the model stomata are steadily open in white light. At "A" the illumination is switched to equal intensity pure red light, and the model stomata begin oscillating with large amplitude. At "B" 5% of blue light replaces 5% of the red, keeping total energy intensity constant. Subsequently, the oscillations diminish.

These behaviors are caused in the SNM by guard cells having a strong intrinsic "blue light" response. When blue light is removed at "A" the immediate guard cell effect is to lose dissolved ions, causing the guard cell water potential to increase and stomatal aperture to close. This subsequently decreases the internal CO_2 concentration. That, in turn, leads to an increase in "signal" from the mesophyll that reopens the aperture. This pattern then repeats. When blue light is turned on at "B", the guard cells' intrinsic blue light response keeps the guard cell ion concentration more constant and diminishes the oscillation amplitude.

1.6.4. *Synchronized Stomatal Oscillations in Darkness.* Under some conditions, the stomata of at least some plants are slightly

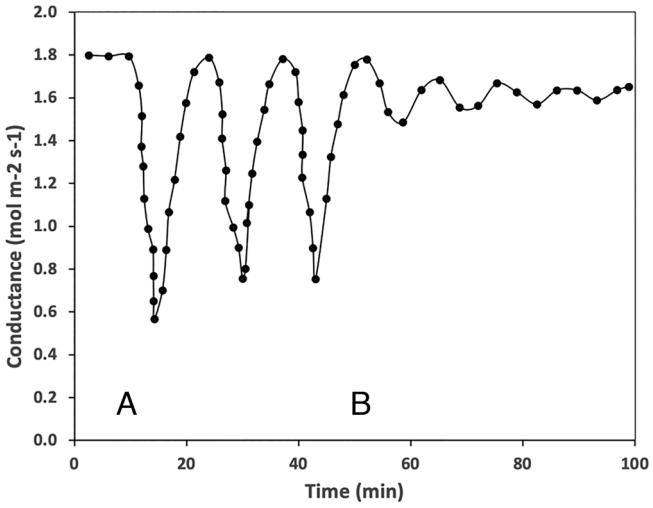

Fig. 4. Simulation of the "red-blue" response.

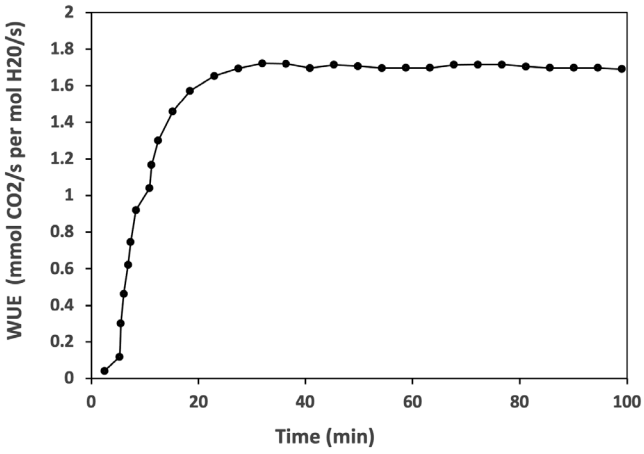

Fig. 6. Simulation of water use efficiency

open in the dark. When that occurs, gas exchange measurements sometime show that the stomata persistently oscillate together (17, 18). Such oscillations thus imply that the openings and closings of many stomata are at least partially synchronized. If, in the SNM, the stomatal pores are initially open in the dark, the model also exhibits small, synchronized, persistent, and rapid stomatal oscillations.

This is shown in the SNM simulation in Fig. 5. The data points on the plot represent stomatal conductance averaged over a leaf surface in the SNM. When a stoma is open in the dark in the SNM, small amplitude oscillations result from small temperature and associated water potential oscillations. Water sharing between adjacent (but randomly slightly different) stomata results in the noisy synchronization shown in the figure. To emphasize that the data have a strong periodic content, the solid superposed curves in Fig. 5 are of the form $\bar{g}_{Sw}(t) = 0.15 + 0.05\sin[\frac{2\pi(t - t_{data})}{4.22}]$, where t_{data} is the time of an SNM (noisy) data point (i.e., the period is 4.22 min).

1.6.5. ***Water Use Efficiency.*** Fig. 6 depicts the time course of the SNM simulation of water use efficiency. WUE on the graph is the ratio of the rate at which carbon dioxide is acquired to the rate at which water is lost through open stomata. At first, the model stomata are closed in the dark. After light is turned on stomata open (as shown in Fig. 2) and WUE increases. Eventually, WUE reaches an approximate asymptotic value, which is presumably a maximum for the specific plant and the starting environmental conditions.

Because WUE is the ratio of CO_2 flux-in to H_2O flux-out through the *same average* stomatal openness, it might be expected that WUE would be essentially independent of time. The time course of WUE subsequent to turning on light has been observed in multiple plant species (19), and each such measurement shows a similar steep rise followed by a plateau, as in Fig. 6. Researchers in these studies speculate that the delayed onset of CO_2 assimilation after light is turned on might arise from some (unknown) biochemical process. The SNM provides a simpler, physical, alternative perspective.

In the SNM the growth of stomatal patchiness and increased water use efficiency are strongly correlated. In Fig. 6 water use efficiency is very low shortly after a leaf is exposed to bright light. In that condition, the stomatal configuration on the leaf is similar to what is depicted in the left image in Fig. 2—i.e., a random scrambling with no large patches. As patchiness grows—for example, as in the right image in Fig. 2—so too does water use efficiency, as shown for later times in Fig. 6.

WUE increases with patchiness in the SNM because, consistent with observation, lateral heat transport is small [see Section 3.4]. Thus, in the model, an open stomatal plug adjacent to a closed stomatal plug will release its own water vapor plus some from the higher concentration vapor of its closed neighbor. (CO_2 uptake, on the other hand, only depends on the open plug.) The vapor gradient is not eliminated by heat transport. On the other hand, an open plug surrounded by other open plugs won't have a vapor gradient and won't release extra water. Consequently, a large patch of contiguous open stomatal plugs (as in the right image of Fig. 2) will release less total water—and therefore produce increased WUE—than an equal number of open plugs interspersed with neighboring closed plugs (as, e.g., in the left image in Fig. 2).

It is interesting to note that the emergence of patchiness in the SNM occurs only when adjacent epidermal cells easily exchange liquid water with one another, that is, when the model parameter $\eta_{ee} \approx 1/4$ (i.e., "strong" epidermal cell water exchange). If, on the other hand, $\eta_{ee} \approx 0$ ("weak" water exchange), no large patches form. In the latter case, the small scale irregularity in the initial open-closed configuration persists and so does low water use efficiency. Thus, the results of the SNM might be interpreted as due to the evolution, for different plants, of increased water exchange between slightly irregularly shaped epidermal cells. In this view, the ubiquity of stomatal patchiness shouldn't be "puzzling;" patchiness is what should be expected to occur.

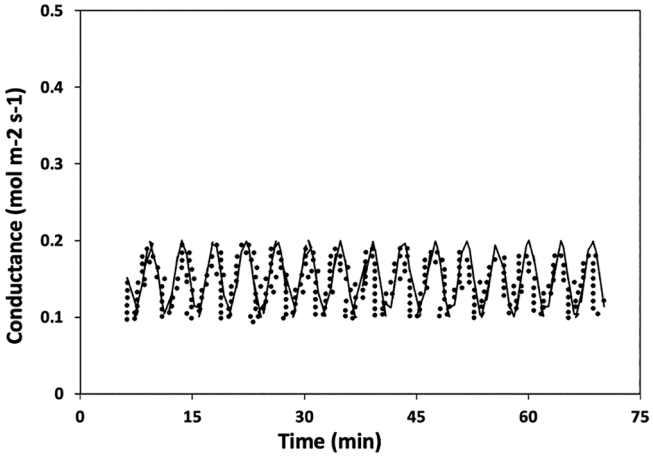

Fig. 5. Simulation of oscillations in darkness

2. Two-Layer, Adaptive, Cellular Nonlinear Networks and Implications for Stomata

A two-layer, adaptive, cellular nonlinear network paradigm was proposed in 2007 by Koeppl and Chua (10). Their model is a computational network of electronic "cells," each of which is capable of changing its internal voltage depending on its instantaneous value as well as the voltages of the cells to which it is wired. Each cell broadcasts its internal voltage (via current exchange) to its *nearest neighbors* only. In the adaptive version, each layer of cells can receive signals from external sources. Depending on the program being executed, each cell can change its internal voltage according to its present voltage and all of its input voltages, and subsequently broadcast the result to the cells to which it is connected. Eventually, this activity settles into a steady (or steadily oscillating) state, which corresponds to "an answer" to the problem being solved. In this version, the problem to be solved can change when the external inputs change; that is, the network can "adapt."

The dynamical equations in the Koeppl and Chua (K-C) adaptive CNN are summarized by

$$\frac{dx^l(r,t)}{dt} = -\lambda_l x^l(r,t) + A^l\left[u\left(r',t\right),\ r\right]\cdot y^l\left(r',t\right) + \sum r'\, B^l\left[u\left(r',t\right),\ r\right]\cdot u^l\left(r',t\right) + z^l(r,t). \quad [4]$$

Here: $x^l(r,t)$ is the internal voltage of the cell at position $r = i,j$ and time t in layer l = 1 or 2; $y^l(r,t)$ is the output voltage of the cell at position $r = i,j$ and time t in layer l; $y^l(r,t) = F[x^l(r,t)]$, where F is a *trilinear function* of its argument; $u^l(r,t)$ is a function of the external inputs to the cell at position r and time t in layer l; the sums are over all the nearest neighbor positions of r, as well as r itself; λ_l is a "relaxation" rate constant for cells in layer l; the As and Bs are functions of the external inputs (thus, allowing for adaptability); $z^l(r,t)$ is the "bias" of the cell at r and time t in layer l.

The dynamical Eqs. **3a** and **3b** for the SNM can be understood as such an adaptive CNN, with the indices e and g corresponding to the leaf's two "computational layers." Identifying the various SNM terms in Eqs. **3a** and **3b** with those in the K-C bilayer adaptive CNN (4) yields:

For the e –computational layer:

- $P_e \leftrightarrow$ the CNN state x^1;
- $\lambda_e \leftrightarrow$ the CNN relaxation rate constant λ_1;
- $\lambda_e\{-\rho g_{Sw}(r,t)\left[w_m(r,t) - w_a\right]\} \leftrightarrow$ the CNN A^1 term;
- $\lambda_e\left[\Gamma_e(r,t)RT_e(r,t) - \eta_{ee}\sum_{r'}\Gamma_e\left(r',t\right)RT_e\left(r',t\right)\right] \leftrightarrow$ the CNN B^1 term;
- $\lambda_e\eta_{ee}\sum_{r'}P_e\left(r',t\right) \leftrightarrow$ the CNN z^1 term.

For the g –computational layer:

- $P_g \leftrightarrow$ the CNN state x^2;
- $\lambda_g \leftrightarrow$ the CNN relaxation rate constant λ_2;
- $\lambda_g\left[\Gamma_g(r,t)RT_e(r,t) + \frac{RT_e(r)}{v_W}\ln\left(\frac{w_c(r,t)}{w_{sat}(r,t)}\right)\right] \leftrightarrow$ the CNN B^2 term;
- the CNN A^2 and z^2 terms are zero.

The stomatal network system described in the preceding sections is therefore structurally identical to a two-layer, adaptive, cellular nonlinear network that performs analog computation. This argument constitutes an exact identification of plant behavior with computation—and thus precisely supports the proposals that plants might be said to compute found in refs. 3–9.

While the latter conclusion is conceptually interesting, there is a potentially more important consequence: the arrows in the identifications above go both ways. Thus, irrespective of whether or not stomata compute, it is certainly the case that adaptive, cellular nonlinear networks can be made to model stomatal networks. That is, when the CNN rate constants and term factors are suitably parametrized with relevant plant values, a CNN can simulate the corresponding leaf's stomatal network behavior. Therefore, a CNN can be used to rapidly perform large numbers of "what-if" experiments with sequentially altered input parameters, investigating "yields and properties" of possibly hitherto unknown "plant behaviors." Such a research program will probably require a significant investment in resources (adaptive CNNs can't be bought off the shelf, they have to be constructed individually for each user) and will likely involve collaboration between plant scientists and computer scientists/engineers. If successful, such a program will determine which CNN parameters lead to improved numerical outputs. These, in turn, should be useful for suggesting possible genetic modification and/or environmental control techniques to investigate improved crop yields, water use, and other potentially desirable characteristics of plants in the real world.

3. Appendix: The Various Details Underlying Eqs. 3a and 3b

The equations developed below tacitly assume that changes in external factors are sufficiently small that possible chemical effects due to plant hormones, for example, can be ignored.

3.1. Rates of Change of Turgor Pressure. Cellular turgor pressure varies with a cell's water content. When free to do so, water flows from higher *water potential* to lower. Thus, the turgor pressure in the guard cells at site r varies in time as

$$\frac{dP_g(r,t)}{dt} = \lambda_g\left[\Psi_c(r,t) - \Psi_g(r,t)\right], \quad [A1]$$

where Ψ_g is the water potential of the liquid inside the guard cells and Ψ_c is the water potential of the vapor in the stomatal cavity adjacent to the guard cells (20); λ_g is the rate constant for water transport in and out of guard cells. (In the SNM presented here, guard cells exchange water only with the vapor in their adjacent stomatal cavity.)

Similarly, the turgor pressure in the epidermal cells on the abaxial surface of the leaf (i.e., where the stomata are) at site r varies in time as

$$\frac{dP_e(r,t)}{dt} = \lambda_e\left[\{\Psi_m(r,t) + \eta_{ee}\sum_{r'}\Psi_e(r',t)\} - \Psi_e(r,t)\right]. \quad [A2]$$

In this expression, Ψ_m is the water potential of the liquid on the mesophyll cells; Ψ_e is the water potential of the liquid inside epidermal cells; the r's are the sites of the nearest neighbors of r; and η_{ee} is a measure of the strength of water sharing between abaxial epidermal neighbors.

3.2. Water Potentials. If the liquid water potential at the *source* (the petiole for a detached leaf, the roots for a potted plant) is defined as $\Psi_S = 0$, then the liquid water potential at the mesophyll is

$$\Psi_m(r,t) = -\rho E(r,\ t), \quad [A3]$$

where $E(r,\ t)$ is the transpiration rate at time t from the stoma at r, and ρ is the resistance to liquid water flow from the source to the leaf interior.

The liquid-phase water potentials within the epidermal and guard cells are the respective differences between turgor (P) and osmotic (Π) pressures. The osmotic pressures are of the form $\Pi_x(r,t) = \Gamma_x(r,t)RT(r,t)$, where $\Gamma_x(r,t)$ is the relevant (i.e., $x = e$ or g) ionic concentration at r, t; R is the universal gas constant; and $T(r,t)$ is the leaf temperature in Kelvins at r, t. Thus, for both epidermal and guard cells,

$$\Psi_x(r,t) = P_x(r,t) - \Gamma_x(r,t)RT(r,t). \qquad [\mathbf{A4}]$$

In general, the water potential of a vapor of arbitrary water content in air—with mole fraction $w(r,t)$ —in equilibrium with liquid water at temperature T is given by

$$\Psi[T(r,t)] = \frac{RT}{V_W}\ln[\frac{w(r,t)}{w_{sat}[T(r,t)]}], \qquad [\mathbf{A5}]$$

where V_W is the molar volume of pure water and $w_{sat}[T(r,t)]$ is the saturated water vapor mole fraction over liquid water at temperature $T(r,t)$.

3.3. Ionic Concentrations. In the SNM, the ionic concentration in solution within all epidermal cells is taken to be time independent, i.e., $\Gamma_e(r,t) = \Gamma_{e0}$. On the other hand, the ionic concentration in solution within guard cells is—like the epidermal cells—partly fixed by metabolism, Γ_{g0}, but also varies with the color and intensity of the incident light. In particular, guard cells have an intrinsic response to absorbed blue light and, in addition, receive—and respond to—a light-related "signal" generated by light absorbed in the mesophyll (20–24). Thus, in the SNM, the ionic concentration in solution within the guard cells is

$$\Gamma_g(r,t) = \Gamma_{g0} + \Gamma_b(r,t) + \Gamma_s(r,t), \qquad [\mathbf{A6}]$$

where $\Gamma_b(r,t) = \Gamma_{b0}\frac{I_b}{I_b + K_b}$ and $\Gamma_s(r,t) = \Gamma_{s0}\frac{I_0}{I_0 + K_s c_i(r,t)}$.

In Eq. **A6**, I_b is the blue light energy intensity and I_0 is the total light energy intensity (both assumed to be spatially uniform in experiments) at site r and time t, and the K's are appropriate rate constants. The quantity $c_i(r,t)$ is the instantaneous mole fraction of gaseous carbon dioxide within the leaf at r, t. The SNM assumes that the amount of "signal" delivered to the guard cells is proportional to the light energy absorbed in the mesophyll but *not* used in photosynthesis (20–24). For a given intensity of light, therefore, the less (alternatively, more) CO_2 available, the more (less) signal is produced. This causes the water potential in the guard cells to decrease (increase) and therefore water to enter (exit), and, as a result, the stomatal aperture to increase (decrease).

3.4. Temperature. Experiments equipped with high resolution thermal imaging capability often observe large patches of different temperatures moving *coherently* on a leaf's surface over time scales of minutes. Sometimes such patches can persist for hours. This suggests that lateral thermal conductivity on the surface of and within a leaf is small. Therefore, the energy balance at site r involving the leaf, the surrounding air, and the incident light leads to a unit-average *local leaf temperature* of the form

$$T(r,t) = T_a + \frac{\delta \cdot I_0 - L_W E(r,t)}{K_a}, \qquad [\mathbf{A7}]$$

where T_a is the air temperature, δ is the fraction of the incident light intensity, I_0, absorbed by the mesophyll that is dissipated as heat, $L_W E(r,t)$ is the rate of cooling of a unit due to transpiration (L_W is the latent heat of water vaporization), and K_a is the thermal conductivity of air. (Thermal radiation at typical air temperatures is assumed to be small.)

3.5. Water Vapor. The water vapor inside the leaf adjacent to the mesophyll is assumed to be saturated (25) at the temperature given by Eq. **A7** above. The water potential at the mesophyll is given by Eq. **A3** above, but, for most laboratory conditions, at least, is approximately 0. In that case, the mole fraction of the saturated vapor at the mesophyll is the usual saturated vapor pressure at the temperature $T(r,t)$: $w_m(r,t) = w_{sat}[T(r,t)]$.

If the stomatal pore is open, water vapor diffusion from the mesophyll to the surrounding air requires that the water vapor mole fraction in the stomatal cavity be less than $w_m(r,t)$. A reasonable assumption is

$$w_c(r,t) = \sigma w_a + (1-\sigma)\Big[(1-4\epsilon)w_m(r,t) + \epsilon \sum w_m\big(r',\mathrm{t}\big)\Big] \qquad [\mathbf{A8}]$$

where w_a is the water vapor mole fraction in the surrounding air and σ is a small fraction (20) (zero, if the pore is closed). The terms multiplied by ϵ (another small fraction) represent water sharing (if any) in the vapor between adjacent stomatal units. With this approximation, the transpiration rate from site r is

$$E(r,t) = g_{Sw}(r,t)\big[w_c(r,t) - w_a\big]. \qquad [\mathbf{A9}]$$

Though small, σ determines how the water potential in the stomatal cavity varies with the humidity in the air, and this in turn affects the guard cell turgor pressure (through Eq. **A1**)—and therefore the stomatal conductance, $g_{Sw}(r,t)$.

3.6. Carbon Dioxide. As discussed with respect to Eq. **A5** above, the ionic concentration in the liquid solution in the guard cells varies with the concentration of carbon dioxide in the air inside the leaf. To determine the latter requires a kinetics equation describing the leaf processes involving CO_2.

It is well established that stomatal movements are much slower than photosynthetic-related processes (26). Thus, the CO_2 kinetics equation can be taken to be in steady state compared with pressure changes of guard and epidermal cells due to water exchange. Consequently,

$$\begin{aligned} 0 = {} & g_c(r,t)\big[c_a - c_i(r,t)\big] - k_c c_i(r,t) I_0 \\ & + \lambda_c[\frac{1}{4}\sum_{r'} c_i\big(r',t\big) - c_i(r,t)]. \end{aligned} \qquad [\mathbf{A10}]$$

The terms in Eq. **A10** describe how the carbon dioxide in the interior of a stomatal unit participates in different interactions. The first term on the RHS represents the diffusive uptake of CO_2 from the air. The second term approximates how gaseous CO_2 is incorporated into photoproducts. (*Technical note: Our CO_2 assimilation estimates rely on the assumption of approximate linearity between A and Ci over the range of Ci in our "experiments." This approximation is reasonable as long as Rubisco limits photosynthesis over the range of Ci values in the simulations. The Ci value at which Rubisco ceases to be limiting and RuBP generation becomes limiting is strongly dependent on species and growth conditions, but because our simulations were done at high light intensity, it is reasonable to*

assume that Rubisco will be limiting over the range of Ci values associated with the simulations, at least for C3 species.) The third term in Eq. **A10** relates to the possible exchange of gaseous CO_2 between neighboring stomatal units. Eq. **A10** can be rearranged to yield

$$c_i(r,t) = \frac{g_c(r,t)c_a + \lambda_c \frac{1}{4}\sum_{r'} c_i(r',t)}{g_c(r,t) + k_c I_0 + \lambda_c}. \qquad [\mathbf{A11}]$$

In Eqs. **A10** and **A11**, $g_c(r,t) = 0.6 g_{Sw}(r,t)$, due to the larger mass of CO_2 relative to H_2O.

All of the phenomena described in the subsections of this Appendix are incorporated in Eqs. **3a** and **3b**.

The Python code and numerical values of the associated parameters used in the simulations shown in Figs. 2–6 can be found at https://github.com/MHogan17/LeafModel.

Data, Materials, and Software Availability. All study data are included in the article and/or main text. There are no data underlying this work.

1. J. J. Hopfield, Neural networks and physical systems with emergent collective computational abilities. *Proc. Nat. Acad. Sci. U.S.A.* **79**, 2554–2558 (1982).
2. J. P. Crutchfield, M. Mitchell, The evolution of emergent computation. *Proc. Nat. Acad. Sci. U.S.A.* **92**, 10742–10746 (1995), 10.1073/pnas.92.23.10742.
3. A. Trewavas, Green plants as intelligent organisms. *Trends Plant Sci.* **10**, 413–419 (2005).
4. S. Karpiński, M. Szechyńska-Hebda, Secret life of plants, from memory to intelligence. *Plant Signal. Behav.* **5**, 1391–1394 (2010), 10.4161/psb.5.11.13243.
5. D. Chu, M. Prokopenko, J. Christian, J. Ray, Computation by natural systems. *Royal Soc. Int. Focus* **8**, 20180058 (2018).
6. G. W. Bassel, Information processing and distributed computation in plant organs. *Trends Plant Sci.* **23**, 994–1005 (2018), 10.1016/j.tplants.2018.08.006.
7. A. G. Parise, M. Gagliano, G. M. Souza, Extended cognition in plants: Is it possible? *Plant Signal. Behav.* **23**, 994–1005 (2020), 10.1080/15592324.2019.1710661.
8. D. Peak, J. D. West, S. M. Messinger, K. A. Mott, Evidence for complex, collective dynamics and emergent, distributed computation in plants. *Proc. Nat. Acad. Sci. U.S.A.* **101**, 918–922 (2004), 10.1073/pnas.0307811100.
9. K. A. Mott, D. Peak, Stomatal patchiness and task-performing networks. *Ann. Bot.* **99**, 219–226 (2006), 10.1093/aob/mcl234.
10. H. Koeppl, L. O. Chua, "An adaptive cellular nonlinear network and its application". *Proceedings of NOLTA'07* (2007), pp. 15–18.
11. K. A. Mott, F. Denne, J. A. Powell, Interactions among stomata in response to perturbations in humidity. *Plant Cell Environ.* **20**, 1098–1107 (1997), 10.1046/j.1365-3040.1997.d01-138.x.
12. J. D. West, D. Peak, J. Q. Peterson, K. A. Mott, Dynamics of stomatal patches for a single surface of *Xanthium strumarium* L. leaves observed with fluorescence and thermal images. *Plant Cell Environ.* **28**, 633–641 (2005), 10.1111/j.1365-3040.2005.01309.x.
13. I. R. Cowan, Oscillations in stomatal conductance and plant functioning associated with stomatal conductance: Observations and a model. *Planta* **106**, 185–219 (1972).
14. W. Beyschlag, J. Eckstein, Stomatal patchiness. *Prog. Bot.* **60**, 283–298 (1998).
15. J. W. Haefner, T. N. Buckley, K. A. Mott, A spatially explicit model of patchy stomatal responses to humidity. *Plant Cell Environ.* **20**, 1087–1097 (1997).
16. Y. Zait, O. Shapira, A. Schwartz, The effect of blue light on stomatal oscillations and leaf turgor pressure in banana leaves. *Plant Cell Environ.* **40**, 1143–1152 (2017), 10.1111/pce.12907.
17. K. A. Mott, D. Peak, Stomatal responses to humidity and temperature in darkness. *Plant Cell Environ.* **33**, 1084–1090 (2010), 10.1111/j.1365-3040.2010.02129.x.
18. P. B. Reich, Oscillations in stomatal conductance of hybrid poplar leaves in the light and dark. *Physiol. Plant.* **61**, 541–548 (1984), 10.1111/j.1399-3054.1984.tb05167.x.
19. L. McAusland *et al.*, Effects of kinetics of light-induced stomatal responses on photosynthesis and water-use efficiency. *New Phytol.* **211**, 1209–1220 (2016), 10.1111/nph.14000.
20. D. Peak, K. A. Mott, A new, vapour-phase mechanism for stomatal responses to humidity and temperature. *Plant Cell Environ.* **34**, 162–178 (2010), 10.1111/j.1365-3040.2010.02234.x.
21. G. D. Farquhar, S. C. Wong, An empirical model of stomatal conductance. *Australian J. Plant Physiol.* **11**, 191–210 (1984).
22. K. A. Mott, D. G. Berg, S. M. Hunt, D. Peak, Is the signal from the mesophyll to the guard cells a vapour-phase ion? *Plant Cell Environ.* **37**, 1184–1191 (2013), 10.1111/pce.12226.
23. Takashi Fujita, Ko. Noguchi, Ichiro Terashima, Apoplastic mesophyll signals induce rapid stomatal responses to CO2 in Commelina communis. *New Phytol.* **199**, 395–406 (2013), 10.1111/nph.12261.
24. Takashi Fujita, Ko. Noguchi, Hiroshi Ozaki, Ichiro Terashima, Confirmation of mesophyll signals controlling stomatal responses by a newly devised transplanting method. *Funct. Plant Biol.* **46**, 467–481 (2019), 10.1071/FP18250.
25. G. D. Farquhar, I. R. Cowan, Oscillations in stomatal conductance. The influence of environmental gain. *Plant Physiol.* **54**, 769–772 (1974).
26. T. Lawson, M. R. Blatt, Stomatal size, speed, and responsiveness impact on photosynthesis and water use efficiency. *Plant Physiol.* **164**, 1556–1570 (2014), 10.1104/pp.114.237107.